Western European cold spells in current and future climate

Hylke de Vries,[1] Reindert J. Haarsma,[1] and Wilco Hazeleger[1]

Received 16 December 2011; revised 30 January 2012; accepted 30 January 2012; published 28 February 2012.

[1] This paper discusses western European cold spells (where temperature falls below the 10% quantile of the winter temperature distribution) in current and future climate. It is demonstrated that many of the projected future changes in cold-spell statistics (duration, return period, intensity) can be explained by changes in the mean (increase) and variance (decrease) of the winter temperature distribution. After correcting for these changes (by subtracting the mean temperature and by dividing by the standard deviation), future cold-spell statistics display no major changes outside estimated error bounds. In absolute terms however, the future cold spells are projected to become ∼5°C warmer (and remain above freezing point), thus having a significant climatic impact. An important contributor to the projected future decrease of temperature variance is shown to be the reduction of the mean zonal temperature gradient (land-sea contrast). These results have been obtained using a 17-member ensemble of climate-model simulations with current and future concentration of greenhouse gases. **Citation:** de Vries, H., R. J. Haarsma, and W. Hazeleger (2012), Western European cold spells in current and future climate, *Geophys. Res. Lett.*, *39*, L04706, doi:10.1029/2011GL050665.

1. Introduction

[2] This paper focuses on statistics of cold spells (CS) defined as days in which the temperature falls below a percentile of the winter probability density function (pdf), and how they might change as a result of climate change. It is well known that the warming of the European continent as a result of climate change will be non uniform [e.g., *Klein Tank et al.* 2005]. Land areas will warm more rapidly than sea areas [*Joshi et al.*, 2008], and high latitudes more than lower latitudes. In addition, many climate models exhibit a modification of the mean westerly circulation [*van Ulden and van Oldenborgh*, 2006]: its strength increases while simultaneously becoming more zonally oriented. Both changes affect temperature variability and therefore, possibly also CS.

[3] Studies have shown that even in a warming climate, long-lasting periods where temperatures drop below an absolute threshold (e.g. frost days), may still be produced locally and occasionally [see, e.g., *Kodra et al.*, 2011]. However, the frequency and average duration of such events will eventually decrease [e.g., *Russo and Sterl*, 2011]. It is less clear whether the above mentioned changes also occur if one adopts a percentile threshold with respect to a non-stationary reference climate. This is investigated in the present study.

[4] Since processes driving potential changes in temperature variability are likely to be season-dependent, we base the analysis of CS statistics on the wintertime pdf. *Ballester et al.* [2010] (BGR10) have already shown that many quantiles of the future annual temperature distribution can be derived from a present-day "control" pdf by adjustment of the mean, standard deviation and skewness. Apart from basing the analysis on a different pdf, we also discuss CS statistics not reported in BGR10. In addition, an attribution study is conducted to relate changes in temperature variability to changes in large-scale parameters such as the zonal temperature gradient, the strength of the westerly circulation and atmospheric blocking.

[5] The paper is structured as follows. After describing data and methodology (section 2), an analysis is given of present-day and future temperature climatology (section 3). The impact of the changes of mean and variability on CS is discussed in section 4. Finally, section 5 attempts to attribute temperature-variability changes to changes in large-scale parameters.

2. Methodology

2.1. Data Preprocessing and Target Area

[6] Data is used from the ERA-40 reanalysis project [*Uppala et al.*, 2005], as well as from the Essence project [*Sterl et al.*, 2008]. The Essence data set is a 17-member ensemble of 150-year integrations obtained with one climate model (ECHAM5/MPI-OM) for the period 1950–2100, assuming the SRES A1b emissions scenario beyond the year 2000. The members were generated by perturbing the initial state of the atmosphere. Results are also given for a multi-model experiment based on the CMIP3 archive [*Meehl et al.*, 2007].

[7] Daily-mean values of 2-meter temperature, mean sea-level pressure and geopotential height at 500 mbar (Z500) have been computed from 6-hourly (ERA-40) and 3-hourly (Essence) fields. The data has been interpolated to a 2.5 degree regular longitude/latitude grid. A 5-day running average has also been used prior to any further operation, to remove short-term fluctuations. Two periods of Essence are considered: 1960–1999 (ESS-NOW) and 2060–2099 (ESS-FUT). The target area of this study is 5E-10E and 50N-55N, which is a region of strong zonal temperature gradient.

2.2. Definitions

[8] A cold day is defined as a day in which the 5-day average temperature in the target area falls below a threshold value T_{cold}. For T_{cold} we use $P10$, the 10% quantile of the non-detrended DJF pdf (of 5-day average temperature) for current and future climate. If the target area covers multiple grid-boxes, the area-mean is computed before estimating the threshold. A cold spell (CS) is defined as a non-interrupted sequence of cold days.

[1]Royal Netherlands Meteorological Institute, De Bilt, Netherlands.

0094-8276/12/2011GL050665

2.3. Uncertainty Estimation

[9] Several CS statistics are discussed. Confidence intervals for return values (section 4.1) are estimated using two different methods: the δ-method [e.g., *Buehler et al.*, 2011] and non-parametric bootstrap [e.g., *von Storch and Zwiers*, 2003]. For the bootstrap, 1000 artificial data sets are created of the same size as ESS-NOW and ESS-FUT. Each year of each artificial member is created by selecting (with replacement) the duration data from that year from a randomly chosen ensemble member. Generalized extreme value (GEV) distributions [*Wilks*, 2006] are fitted through each bootstrap sample and shading covers a high percentage of the bootstrapped GEV fits. Results from the bootstrap are almost identical to those using the δ-method. Bootstrapping is also used for the other CS statistics assuming that CS occur independently. Not considered is uncertainty in the 10% quantile of the winter pdf itself.

3. Winter Temperature Variability

3.1. Present-Day

[10] Figure 1 compares the winter climatologies of ERA-40 and Essence (ensemble-mean). Mean temperatures μ of ERA-40 and ESS-NOW agree very well (Figure 1, top). The variability patterns are also similar (Figure 1, middle), with temperature standard deviation σ being highest where mean temperatures are lowest. Figure 1 (bottom) displays a scaled version of the T_{cold} pattern, namely $(T_{cold} - \mu)/(\mu - P10_n)$, where $P10_n$ is the 10% quantile of a normal distribution with the same μ and σ. Hence, a value $T_{cold} < -1$ indicates that T_{cold} is colder than $P10$ of a Gaussian pdf. This is the case for most of the continent and is consistent with the pdf being negatively skewed. The agreement between ERA-40 and ESS-NOW is reasonable.

3.2. Future Projections

[11] The future projections show a non-uniform increase of winter mean temperature. High latitudes and the continents warm more than low latitudes and the Atlantic Ocean. Also σ decreases nearly everywhere, but assessing the statistical significance of this change is difficult. While reductions are generally $\sim$20%, the edge of the Arctic experiences decreases of $\sim$50%. Most areas in Europe show no major changes of (scaled) T_{cold}, implying that most of the change in absolute T_{cold} is accounted for by changing μ and σ.

4. Cold-Spell Statistics

[12] Three cold-spell statistics are discussed. First we investigate CS duration return periods for the target area. Then we turn to the typical CS evolution or 'life cycle' and a measure of CS 'intensity', namely the CS mean temperature. Two further statistics for the European area are discussed in the auxiliary material (Figures S2 and S3 in Text S1).[1]

4.1. Duration

[13] GEV distributions are fitted to the duration data, adopting a 4-year block-maxima approach (at least one CS occurred in each block) and using all ensemble members. Figure 2 (left) shows the resulting Gumbel plot [*von Storch and Zwiers*, 2003]. The GEV fits are remarkably similar and the confidence interval of ESS-NOW covers the fits through ERA-40 and ESS-FUT. In the auxiliary material we demonstrate that not only the extremes but the entire duration distribution is very similar (Figure S1 in Text S1).

4.2. Evolution

[14] A composite of CS was created for the target area. The composite consists of non-overlapping CS events, which are centered at the time of minimum temperature. Figure 3 (left) shows the composite evolution from 7 days prior, to 7 days after the temperature minimum. Temperatures gradually drop toward the minimum, which in case of ESS-FUT is $\sim$5°C higher than ESS-NOW. In both cases the CS lasts for 5 to 6 days. After subtracting the difference in mean DJF temperature, the future CS remain significantly warmer (not shown). However, after subsequent dividing by the standard deviation σ of each period, the life cycles become very similar (Figure 3, middle). Subtracting the mean DJF temperature and subsequently dividing by the standard deviation from here on is referred to as 'scaling'. After scaling, the confidence intervals overlap substantially and temperatures reach (on average) more than two σ below μ. Figure 3 (right) shows the scaled composite evolution for a subset of the CMIP3 data set. Despite the fact that the underlying climates of the models differ considerably (see auxiliary material), the scaled composite evolution is very similar. In both Essence and CMIP3 there is a small (but statistically significant) difference for $t > 2$: the future CS recover on average slightly faster from the minimum than in present-day. Further study is required to examine the physical significance of this result.

4.3. Mean Temperature

[15] Figure 2 (middle) shows scaled mean CS temperature as a function of minimal duration. As expected, long-lasting CS are on average colder than short-lived CS. Regressing mean CS temperature on duration reveals that the mean CS temperature drops about 0.35σ in week 1 and less thereafter. At longer duration the uncertainty increases due to the lack of such events within the considered 40-year time periods. As with the life-cycle results, there is no evidence that scaled CS mean temperatures will become very different in future.

4.4. Extremes

[16] The scaling approach appears to work particularly well for the average CS. Here we examine whether the "extreme" CS also become similar after scaling. Figure 2 (right) shows a quantile-quantile plot [*von Storch and Zwiers*, 2003] for scaled CS minimum temperatures of ESS-NOW and ESS-FUT. The scaling appears to be appropriate (i.e., confidence interval overlapping with $y = x$ line) up to the 10% coldest CS. Beyond that level, the scaled future CS are somewhat colder than those of present-day. Further study is required to examine the physical significance of this difference.

5. What Causes the Change of Temperature Variability?

[17] The previous sections showed that after scaling by σ, the CS of the two periods of Essence become similar (except

[1] Auxiliary materials are available in the HTML. doi:10.1029/2011GL050665.

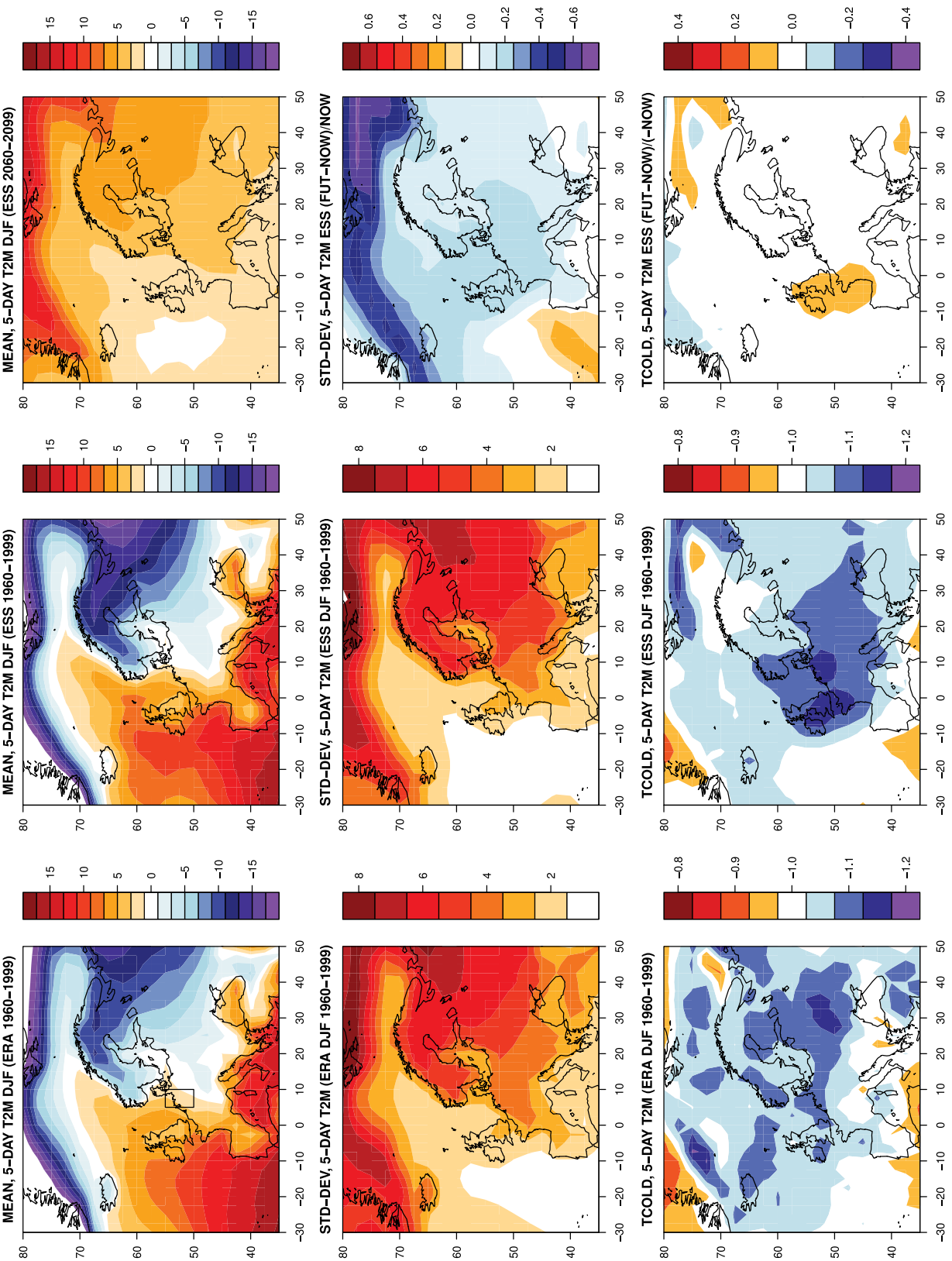

Figure 1. Winter climatology of 5-day running average 2 m-temperature. (left) ERA-40, (middle) ESS-NOW, and (right) difference between ESS-FUT and ESS-NOW. (top) Mean μ [Celsius]. (middle) Standard deviation σ [Celsius]. (bottom) Scaled CS threshold $(T_{cold} - \mu)/(\mu - P10_n)$. The top left plot displays the target area (box).

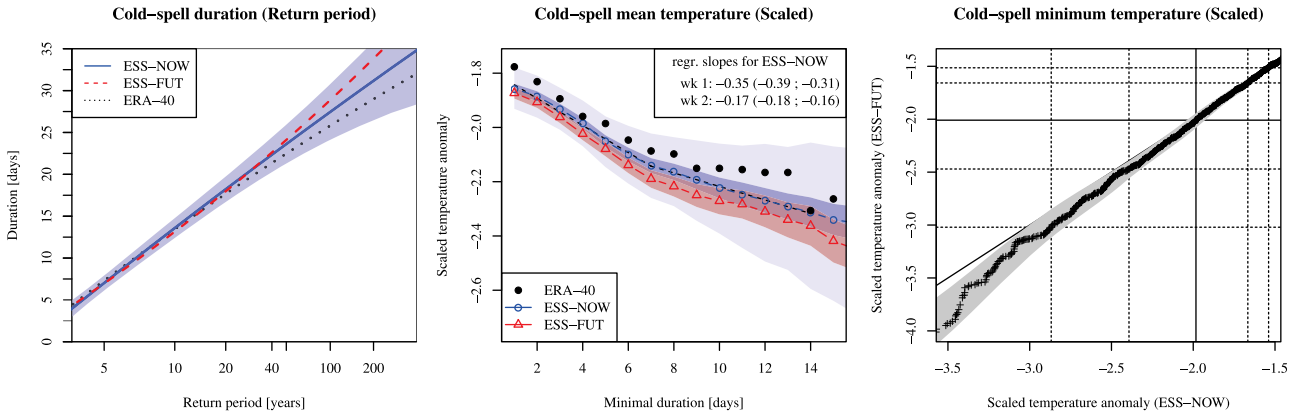

Figure 2. (left) CS duration. Displayed are Gumbel plots of average return period (years) for CS of given duration (days). Confidence interval (95%) for ESS-NOW obtained using δ-method. See section 2.3 for explanation of methods. (middle) Mean CS temperature (scaled) as a function of duration. Regression lines for first (wk1) and second (wk2) week of ESS-NOW are dashed. The dark (light) shading shows 95% confidence intervals resulting from a 17-member (1-member) bootstrap. (right) Quantile-quantile plot for (scaled) CS minimum temperature. Vertical (horizontal) dashed lines indicate quantiles $P10$, $P25$, $P75$ and $P90$ for ESS-NOW (ESS-FUT), while $P50$ is denoted as a full line. Confidence interval (95%) estimated using bootstrap. The line $y = x$ is also shown.

for the coldest extremes, see section 4.4). An important question is therefore what governs the change of σ. Figure 1 shows that the coldest areas are expected to face the strongest warming. This implies that horizontal temperature gradients reduce significantly. With advection being proportional to wind and temperature gradient, and being an important source of temperature variability, it can be anticipated that changes in these components have an immediate impact on temperature variability and therefore on σ. Indeed, a strong reduction of σ is seen in areas where temperature gradients reduce. Here we focus on the changes of σ in the target area, for which the change in zonal temperature gradient is much larger than the change in meridional temperature gradient.

5.1. Linear Statistical Model

[18] A statistical model has been constructed to relate changes of σ to changes in the zonal temperature gradient (denoted Tx) and two circulation indices. The first circulation index is the westerly component of the surface geostrophic wind (Gw) [*van Ulden and van Oldenborgh*, 2006]. Gw is computed for each grid-box using sea-level pressure at the corners of a 20 × 10 degrees lon-lat box centered around that grid-box. Local Gw values are averaged over the target area. The same approach is used to compute Tx from the temperature data. The second circulation index is the blocking index (B) of *Tibaldi and Molteni* [1990]. This index measures large-scale reversal of the climatological gradient of Z500. The index B is computed for standard parameters (only $\Delta = (0, \pm 2.5, \pm 5)$ is taken) and the resulting longitudinal B series is averaged over 0-40E. Monthly-mean values of Gw, B, Tx and σ are obtained for DJF, and subsequently regressed against time. In this way we obtain the 150-year changes (denoted as Δvar). This

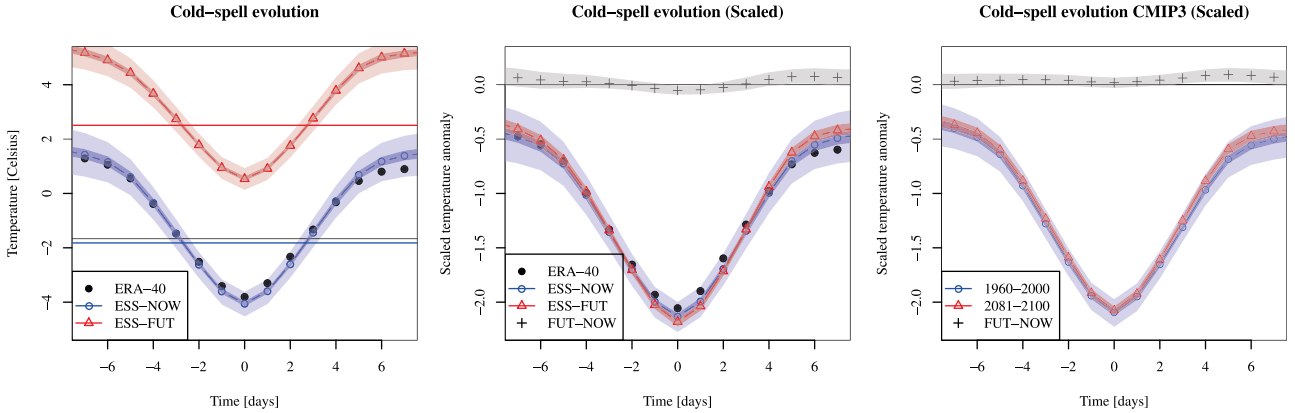

Figure 3. CS evolution. (left) Composite evolution centered at time of minimum. Horizontal lines denote T_{cold}. Confidence intervals estimated using bootstrap. The dark (light) shading indicate confidence intervals (95%) for a 17-member (1-member) bootstrap. (middle) As in the left plot but after scaling. The grey band displays a confidence interval for the difference. (right) As in the middle plot but for CMIP3 data (light shading in this plot denotes a confidence interval derived from a bootstrap with 1/17 of all CMIP3 data).

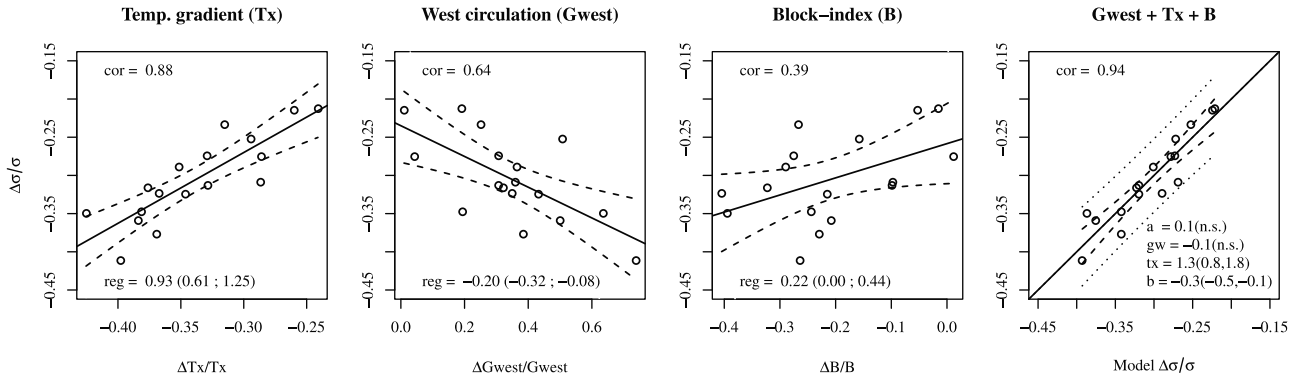

Figure 4. Scatter-plots of Δ-change coefficients against $\Delta\sigma$. Dashed lines show 95% confidence intervals for the regressions, obtained using standard t-test [*von Storch and Zwiers*, 2003]. Components have been scaled by the ensemble-mean of ESS-NOW. The right plot shows the linear statistical model with all components. Dotted lines show 95% confidence interval for prediction using linear model.

process is repeated for each ensemble member separately, resulting in 17 Δ-values per variable. A statistical model is formulated

$$[\Delta\sigma]_{lm} = a + gw(\Delta Gw) + tx(\Delta Tx) + b(\Delta B), \qquad (1)$$

where a, gw, tx and b are parameters to be estimated using multiple linear regression to the observed $\Delta\sigma$.

5.2. Results

[19] Scatter-plots of the variables with $\Delta\sigma$ are shown in Figure 4. Of all three variables, ΔTx has the highest Spearman rank-correlation with $\Delta\sigma$ (0.88). Ensemble members that exhibit a stronger decrease of Tx generally also show a stronger reduction of σ. Similarly a stronger increase (decrease) of Gw (B) concurs with stronger reduction of σ. Figure 4 (right) shows the estimate from the linear model (1), which has a correlation of 0.94 with $\Delta\sigma$. A model without ΔTx yields a correlation of 0.64 with $\Delta\sigma$, thereby suggesting that ΔTx is the most important factor. However, the variables are correlated [cor(ΔTx, ΔGw) = −0.64, cor(ΔTx, ΔB) = 0.70 and cor(ΔGw, ΔB) = −0.40], nor can we exclude the possibility that the Tx is caused by B and Gw.

[20] Inclusion of the two other components involved in temperature advection (the meridional temperature gradient Ty and the southerly component of the surface geostrophic wind) has also been tested. However, neither of these was found to have absolute correlations ≥ 0.15 with $\Delta\sigma$, nor did they increase cor($\Delta\sigma$, $[\Delta\sigma]_{lm}$). This might however be different for different target areas.

6. Conclusion

[21] Changes in the statistics of western European cold spells (CS) are closely linked to changes of the mean DJF temperature μ and the standard deviation σ. Especially the role of σ cannot be neglected. If the CS threshold is set to the non-stationary 10% quantile of the DJF pdf – which is different in future –, CS duration does not change significantly. After rescaling (subtracting μ and dividing by σ), the CS evolution is also very similar (Figure 3). Composites obtained for a subset of the CMIP3 data set show similar results. Only the coldest future CS appear to be somewhat colder after rescaling (Figure 2, right). It is yet unclear whether the statistical differences found at the coldest CS also point to physically significant differences. An important factor for the change of σ in Western Europe is the change in the mean zonal temperature gradient Tx, caused by the different heating rates of continental and maritime areas.

[22] The results appear to be most robust for CS in western and central Europe. Two further CS statistics are investigated for the European area to support this conclusion (Figures S2 and S3 in Text S1). Robustness is gradually lost when the target area increases in size. Since CS do not always occur at the same day on a very large scale, this is to be expected. Furthermore, replacing σ by the non-parametric scale parameter ($P90 - P10$)/2 used by *Klein Tank et al.* [2005] does not alter the conclusions. However, if one scales by the inter-quartile distance iqr = ($P75 - P25$) [*Wilks*, 2006], there remain small differences between present-day and future CS (future CS being too cold).

[23] BGR10 showed that if one considers absolute temperature thresholds based on current climate, many quantiles of the future temperature pdf can be obtained by modifying the first three moments of the annual pdf. They emphasized that the change of skewness is crucial to explain the changes in the cold tails. The present paper has shown that, at least for the target area under consideration, the first two central moments suffice if one uses the winter pdf. This is an advantage since there is no unique skewness-transformation. Separating summer from winter season also makes sense physically. In summer for example, the stronger heating of the continent leads to an enhanced land-sea contrast, whereas in winter the land-sea contrast is reduced. With temperature advection being an important source of temperature variability, these differences will be reflected in the changes of the temperature pdf. Indeed some of the changes of the temperature pdf (e.g., variance and skewness) display opposite trends in summer and winter in certain areas of Europe [*Klein Tank et al.*, 2005]. The implications for impact studies and statistical downscaling are that by incorporating changes of just mean and standard deviation (assuming they can be diagnosed accurately) many aspects of future CS over western Europe can be realistically simulated based on current climate. However, with CS temperatures increasing with ∼5°C for western Europe, the average future CS is expected to remain above freezing point

(Figure 3). This means that the changes in CS will have a significant climatic impact.

[24] **Acknowledgments.** The authors thank Tim Woollings, Frank Selten and Andreas Sterl for useful discussions. The research has been supported by GasTerra and NAM.

[25] The editor thanks two anonymous reviewers for their assistance evaluating this manuscript.

References

Ballester, J., F. Giorgi, and X. Rodo (2010), Changes in European temperature extremes can be predicted from changes in PDF central statistics, *Clim. Change*, *98*, 277–284, doi:10.1007/s10584-009-9758-0.

Buehler, T., C. C. Raible, and T. F. Stocker (2011), The relationship of winter season North Atlantic blocking frequencies to extreme cold or dry spells in the ERA-40, *Tellus A*, *63*(2), 212–222, doi:10.1111/j.1600-0870.2010.00492.x.

Joshi, M. M., J. M. Gregory, M. J. Webb, D. M. H. Sexton, and T. C. Johns (2008), Mechanisms for the land/sea warming contrast exhibited by simulations of climate change, *J. Clim.*, *30*, 455–465.

Klein Tank, A. M. G., G. P. Können, and F. M. Selten (2005), Signals of anthropogenic influence on european warming as seen in the trend patterns of daily temperature variance, *Int. J. Climatol.*, *25*, 1–16.

Kodra, E., K. Steinhaeuser, and A. R. Ganguly (2011), Persisting cold extremes under 21st-century warming scenarios, *Geophys. Res. Lett.*, *38*, L08705, doi:10.1029/2011GL047103.

Meehl, G. A., C. Covey, K. E. Taylor, T. Delworth, R. J. Stouffer, M. Latif, B. McAvaney, and J. F. B. Mitchell (2007), The WCRP CMIP3 multimodel dataset: A new era in climate change research, *Bull. Am. Meteorol. Soc.*, *88*, 1383–1394, doi:10.1175/BAMS-88-9-1383.

Russo, S., and A. Sterl (2011), Global changes in indices describing moderate temperature extremes from the daily output of a climate model, *J. Geophys. Res.*, *116*, D03104, doi:10.1029/2010JD014727.

Sterl, A., C. Severijns, H. Dijkstra, W. Hazeleger, G. Jan van Oldenborgh, M. van den Broeke, G. Burgers, B. van den Hurk, P. Jan van Leeuwen, and P. van Velthoven (2008), When can we expect extremely high surface temperatures?, *Geophys. Res. Lett.*, *35*, L14703, doi:10.1029/2008GL034071.

Tibaldi, S., and F. Molteni (1990), On the operational predictability of blocking, *Tellus, Ser. A*, *42*, 343–365, doi:10.1034/j.1600-0870.1990.t01-2-00003.x.

Uppala, S. M., et al. (2005), The ERA-40 re-analysis. *Q. J. R. Meteorol. Soc.*, *131*, 2961–3012, doi:10.1256/qj.04.176.

van Ulden, A. P., and G. J. van Oldenborgh (2006), Large-scale atmospheric circulation biases and changes in global climate model simulations and their importance for climate change in central Europe, *Atmos. Chem. Phys.*, *6*, 863–881, doi:10.5194/acp-6-863-2006.

von Storch, H., and F. W. Zwiers (2003), *Statistical Analysis in Climate Research*, 1st ed., Cambridge Univ. Press, Cambridge, U. K.

Wilks, D. S. (2006) *Statistical Methods in the Atmospheric Sciences*, *Int. Geophys. Ser.*, vol. 91, 2nd ed., Academic, London.

H. de Vries, R. J. Haarsma, and W. Hazeleger, Royal Netherlands Meteorological Institute, PO Box 201, de Bilt, NL-3730 AE, Netherlands. (hylke.de.vries@knmi.nl; reindert.haarsma@knmi.nl; wilco.hazeleger@knmi.nl)